Available online at www.sciencedirect.com
SCIENCE DIRECT®
Journal of Solid State Chemistry 177 (2004) 2387–2393
JOURNAL OF SOLID STATE CHEMISTRY
http://elsevier.com/locate/jssc

The effect of a cation radii on structural, magnetic and electrical properties of doped manganites $La_{0.6-x}Pr_xSr_{0.4}MnO_3$

S. Zemni,[a] Ja. Dhahri,[a] K. Cherif,[a] Je. Dhahri,[a,*] M. Oummezzine,[a] M. Ghedira,[a] and H. Vincent[b]

[a] *Département de Physique, Faculté des Sciences de Monastir, Laboratoire de physico-chimie des Matériaux, Monastir 5019, Tunisia*
[b] *Laboratoire des Matériaux et de Génie Physique, ENSPG, B.P. 46, 38402 Saint Martin d'Héres Cedex, France*

Received 8 October 2003; received in revised form 23 February 2004; accepted 7 March 2004

Abstract

Structural, magnetic and transport properties of $La_{0.6-x}Pr_xSr_{0.4}MnO_3$ with $x = 0.0$, 0.03, 0.06, 0.18, 0.3, 0.42, 0.54 and 0.6 are studied. The system exhibits a rhombohedrally distorted ($R\bar{3}c$) perovskite structure for $x \leqslant 0.3$. A rhombohedral–orthorhombic (*Pnma*) structure transition is detected in the doping range from $x = 0.42$ to 0.6. The structure refinement by Rietveld analysis of the X-ray powder diffraction data shows that the average distance Mn–O increases in the rhombohedral phases and decreases in the orthorhombic phases. Results show that the Curie temperature decreases from 374 to 310 K when $\langle r_A \rangle$ varies from 1.254 to 1.231 Å. Electrical measurements show that all samples exhibit a metallic to semiconducting transition with increasing temperature. Meanwhile, the size of the resistivity ρ increases near T_C. This phenomenon is interpreted as a gradual bending of the Mn–O–Mn bond angle, with decreasing $\langle r_A \rangle$, which causes the narrowing of the electronic bandwidth and the effect of the *A*-site variance σ^2.
© 2004 Elsevier Inc. All rights reserved.

Keywords: Perovskite; Manganite; Cation size

1. Introduction

The rare-earth manganites of the type $(Ln^{3+}_{1-x}A^{2+}_x)(Mn^{3+}_{1-x}Mn^{4+}_x)O_3$ where Ln^{3+} is La^{3+}, Pr^{3+}, Nd^{3+} and A^{2+} is Sr^{2+}, Ca^{2+}, Pb^{2+}, Cd^{2+}, Ba^{2+}; have attracted much attention of the scientific community due to the colossal magnetoresistance (CMR) phenomenon and fascinating magnetic system with diverse magnetically ordered structures as one varies the concentration of dopant A [1–3].

The magnetic and transport properties of these samples are determined by several factors such as the percentage of the divalent ions, the ionic radii of the metal ions, the method used in the preparation of the samples, etc. [4,5].

This results in a Mn^{3+}/Mn^{4+} mixed-valence state creating mobile charge carriers and canting of Mn spins [6]. It has been believed that the electrical properties are controlled by the motion of an e_g electron from a Mn^{3+} ($t^3_{2g}e^1_g{:}S = 2$) to Mn^{4+} $\left(t^3_{2g}e^0_g{:}S = \frac{3}{2}\right)$ via the intervening oxygen. The magnetic coupling between Mn^{3+} and Mn^{4+} is also correlated with the motion of the e_g electron between the two partially filled *d*-shells with strong on-site Hund coupling. The electrical and magnetic properties have traditionally been explained within the frame-work of the "double exchange" (DE) theory which considers the magnetic coupling between Mn^{3+} and Mn^{4+} ions [7–10]. The motion of the e_g electron can be strongly influenced by the average ionic radius of the *A*-site $\langle r_A \rangle$ which exhibits a close relationship between the bending of the Mn–O–Mn bond angle and the narrowing of the electronic band width [11,12]. In this paper we report our results of a systematic study of structural, magnetic and electrical properties of compounds with compositions $La^{3+}_{0.6-x}Pr^{3+}_x Sr^{2+}_{0.4}(Mn^{3+}_{0.6}Mn^{4+}_{0.4})O_3$ with $0 \leqslant x \leqslant 0.6$.

From the relationship between the average Mn–O distance and the magnetic and electrical properties, we will make clear the role of the trivalent ion in the ferromagnetic–paramagnetic and metallic–semiconductor transitions.

*Corresponding author.
E-mail address: jemai_dhahri@yahoo.fr (J. Dhahri).

0022-4596/$ - see front matter © 2004 Elsevier Inc. All rights reserved.
doi:10.1016/j.jssc.2004.03.017

2. Experimental procedure

Polycrystalline $La_{0.6-x}Pr_xSr_{0.4}MnO_3$ specimens were synthesized by the conventional solid-state reaction method using Mn/(La + Pr + Sr) ratios equal to 1. The precursors La_2O_3, $SrCO_3$, Pr_2O_3 and MnO_2 of high purity (more than 99.9%) powders were mixed in stoichiometric proportions. Mixtures were first calcined at 1173 K for 72 h in air to achieve decarbonation. After grinding, they were heated at 1273 K for 24 h and reground again to ensure homogenization. After grinding, they were heated again at 1473 K for 24 h in air. Intermediate cooling and mechanical grinding steps were repeated in order to get an accurate homogenization and complete reaction. The powders thus obtained were pressed into pellets under 4 ton/cm^2 and sintered at 1673 K for 4 days in air. Finally, these pellets were rapidly quenched to room temperature in order to avoid the eventual formation of other crystalline phase.

The X-ray powder diffraction patterns were recorded on the Siemens D5000 diffractometer ($\lambda_{CuK\alpha_1} = 1.54056$ Å) and $20° \leqslant 2\theta \leqslant 120°$ with step of 0.02° and counting time of 18 s per step. The structure refinement was carried out by the Rietveld analysis of the X-ray powder diffraction data with FULLPROF software (version 0.2-March 1998-LLB-JRC) [13]. The microstructure was observed by scanning electron microscope (SEM). The pictures were taken at room temperature on a Philips XL30 equipped with a field emission gun at 15 kV.

Magnetization measurements were performed using a home made faraday-type balance for $0 \leqslant x \leqslant 0.6$ and a Foner magnetometer equipped with a super conducting coil in magnetic field of 500 Oe for $x = 0.6$ in low temperature.

The resistivity measurements were carried out by using four-probe method in the earth's magnetic field. The sample was cut into a rectangular shape, with a typical dimension of $5 \times 5 \times 2\,mm^3$.

3. Results and discussions

3.1. SEM

The morphology and particle size of the series $La_{0.6-x}Pr_xSr_{0.4}MnO_3$ are observed with SEM as shown in Fig. 1. A decrease in particle size with increasing Pr content is observed. This seems to indicate that the incorporation of Pr into La-sites inhibits the grain growth during the sintering process at 1673 K.

3.2. Structural properties

All samples are single-phase and have a rhombohedral structure with space group $R\bar{3}c$ for $0 \leqslant x \leqslant 0.3$ that becomes orthorhombic with the space group *Pnma* for $0.42 \leqslant x \leqslant 0.60$. The absence of other peaks demonstrates the solubility of Pr in the perovskite structure.

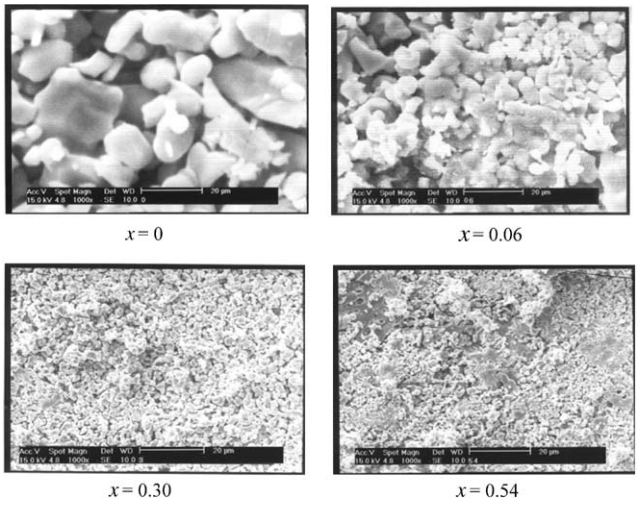

Fig. 1. SEM photographs of $La_{0.6-x}Pr_xSr_{0.4}MnO_3$.

Fig. 2 shows the refinement of $La_{0.6-x}Pr_xSr_{0.4}MnO_3$ ($x = 0.3$ and 0.42) X-ray diffraction diagram obtained at room temperature. The structure refinement of $La_{0.6-x}Pr_xSr_{0.4}MnO_3$ samples was performed in the hexagonal setting of the $R\bar{3}c$ space group, in which the La atoms are at 6*a* (0, 0, 1/4) position, Mn at 6*b* (0, 0, 0) and O at 18*e* $(x, 0, \frac{1}{4})$ with the Pr content $x \leqslant 0.3$ and in the orthorhombic setting of the *Pnma* space group, in which the La atoms are at 4*c* (*x*, 0.25, *z*) position, Mn at 4*b* (0.5, 0, 0) and O_I at 4*c* (*x*, 0.25, *z*) and O_{II} at 8*d* (*x*, *y*, *z*) with the Pr content $x \geqslant 0.42$. The results of refinement are listed in Table 1. In this table, are also reported the residuals for the weighted pattern R_{wp}, the pattern R_p, the structure factor R_F, and the goodness of fit χ^2.

Figs. 3 and 4 show that the cell parameters and the unit cell volume decrease with the praseodymium content. The structural transition in $La_{0.6-x}Pr_xSr_{0.4}MnO_3$ series are governed by the size of the rare-earth ions La^{3+} and Pr^{3+}. The smaller Pr^{3+} ion induces a transformation to orthorhombic symmetry at high values of *x* ($x \geqslant 0.42$). The exact concentrations at which the transformations to orthorhombic symmetry for the Pr series occur are difficult to determine from powder X-ray data. The decrease in the lattice parameters can be related to the narrow size of the Pr ion ($r_{Pr^{3+}} = 1.1791$ Å, and $r_{La^{3+}} = 1.2161$ Å) [14]. This is confirmed by the Rietveld refinement of Mn–O distance calculated from the structural parameters, which also increases with *x* (Table 2). On the other hand, the refined Mn–O–Mn angles are slightly changed by increasing *x* for the rhombohedral phase and decrease significantly in the orthorhombic phase. From the results of the average distances Mn–O and the average angles Mn–O–Mn,

Table 1
Refined structure parameters for $La_{0.6-x}Pr_xSr_{0.4}MnO_3$ after the Rietveld refinements of X-ray powder diffraction data at room temperature

x			0	0.03	0.06	0.18	0.3	0.42	0.54	0.6
	$R\bar{3}c$ phase									
a (Å)			5.4843(9)	5.4832(3)	5.4818(7)	5.4801(2)	5.4757(5)	—	—	—
c (Å)			13.3594(9)	13.3438(5)	13.3369(2)	13.3283(1)	13.3128(2)	—	—	—
V (Å^3)			347.98(4)	347.44(4)	347.09(2)	346.64(3)	345.68(4)	—	—	—
(La/Pr/Sr)	(6*a*)	B (Å^2)	0.569	0.499	0.659	0.244	0.485	—	—	—
(Mn)	(6*b*)	B (Å^2)	0.29(2)	0.42(2)	0.21(2)	0.39(6)	0.16(6)	—	—	—
(O)	(18*e*)	x	0.4657(8)	0.4664(2)	0.4648(3)	0.4604(2)	0.4657(5)	—	—	—
		B (Å^2)	1.33(7)	1.89(4)	1.18(4)	0.96(6)	1.38(6)	—	—	—
	Pnma phase									
a (Å)		—	—	—	—	—		5.4627(2)	5.4544(2)	5.4483(2)
b (Å)		—	—	—	—	—		7.6742(2)	7.6712(3)	7.6681(3)
c (Å)		—	—	—	—	—		5.4922(3)	5.4868(2)	5.4786(7)
V (Å^3)		—	—	—	—	—		230.24(6)	229.57(3)	228.99(5)
(La/Pr/Sr)	(4*c*)	x	—	—	—	—	—	−0.0004(8)	0.0100(1)	0.0116(1)
		z	—	—	—	—	—	−0.0005(3)	−0.0009(9)	−0.0012(4)
		B (Å^2)	—	—	—	—	—	0.31(2)	0.29(6)	0.21(7)
Mn	(4*b*)	B (Å^2)	—	—	—	—	—	0.06(4)	0.14(4)	0.11(3)
O(1)	(4*c*)	x	—	—	—	—	—	0.4821(6)	0.5063(1)	0.5071(2)
		z	—	—	—	—	—	0.0594(2)	0.0438(1)	0.0594(6)
		B (Å^2)	—	—	—	—	—	0.42(4)	0.06(1)	0.48(7)
O(2)	(8*d*)	x	—	—	—	—	—	0.2616(4)	0.2562(3)	0.2636(8)
		y	—	—	—	—	—	0.0256(9)	0.0283(2)	0.0287(6)
		z	—	—	—	—	—	0.7536(1)	0.7461(8)	0.7447(6)
		B (Å^2)	—	—	—	—	—	0.89(5)	1.74(6)	0.42(9)
R_{wp} (%)			13.6	9.5	8.8	10.2	8.97	11.27	10.42	9.6
R_p (%)			10.6	7.9	6.5	6.77	5.59	8.52	6.65	7.44
R_F (%)			2.93	2.66	3.11	2.73	2.88	3.29	2.94	3.49
X^2 (%)			3.87	2.53	3.91	2.69	3.15	4.05	3.64	4.51

it is considered that each BO_6 octahedron has a little distortion.

4. Magnetic properties

Our magnetic measurements reveal that all the samples of $La_{0.6-x}Pr_xSr_{0.4}MnO_3$ oxides are ferromagnetic at low temperature ($T<T_C$) and paramagnetic above the Curie temperature T_C as shown in Fig. 5. The Curie temperature T_C, defined as the temperature corresponding to the inflection point on the $M(T)$ curve is shown in Fig. 6. The transition temperature T_C decreases from 374 to 310 K when the average size $\langle r_A \rangle$ of a site cation decreases from 1.254 to 1.231 Å. In fact, the substitution of La by Pr should not change the Mn^{3+}/Mn^{4+} ratio but the difference in ionic size affects the Mn–O–Mn bond angle. As a consequence, the transfer interaction of e_g electrons should be reduced.

This variation of T_C has been interpreted by the decrease of the Mn–O–Mn bond angles as shown in Table 2 when the $\langle r_A \rangle$ decreases. The average Mn–O–Mn bond angles and the Curie temperature as a function of $\langle r_A \rangle$ for our series of samples are plotted in Fig. 6.

Fig. 7 shows the evolution of the Mn–O–Mn bond angles when the ratio of Pr increases. The Curie temperature T_C is not affected by the variation of $\langle r_A \rangle$ and Mn^{3+}/Mn^{4+} ratio. In fact recent studies of $La_{0.7}A_{0.3}MnO_3$ [15] and $Ln_{0.5}A_{0.5}MnO_3$ [16] reveal that the "mismatch effect factor" influences T_C. This factor is represented by the variance of the A-site cation radii distribution σ^2, defined by the following expression:

$$\sigma^2 = \sum_i x_i r_i^2 - \langle r_A \rangle^2,$$

where r_i corresponds to the radii of the various A-site cations and x_i to their fractional occupancies $\left(\sum_i x_i = 1\right)$.

To confirm this behavior for our samples, we present in Table 3 different values of T_C versus σ^2 for three samples which have the same $\langle r_A \rangle$ equal to 1.248 Å and the same ratio Mn^{3+}/Mn^{4+} equal to 3/2.

On the other hand it has been reported [19,20] that the compounds ($Sm_{0.5-x}La_xSr_{0.5}MnO_3$, $Sm_{0.5-x}Pr_xSr_{0.5}MnO_3$, $Gd_{0.5-x}Pr_xSr_{0.5}MnO_3$, $Y_{0.5-x}Pr_xSr_{0.5}MnO_3$, $Pr_{0.5}Sr_{0.5-x}Ca_xMnO_3$, etc.) where the ratio ($Mn^{3+}/Mn^{4+}=1$) is near from of our samples $La_{0.6-x}Pr_xSr_{0.4}MnO_3$ ($Mn^{3+}/Mn^{4+}=1.5$) exhibit an antiferromagnetic–ferromagnetic transition with a Neel temperature point $T_N \approx 130$ K. To check if this transition

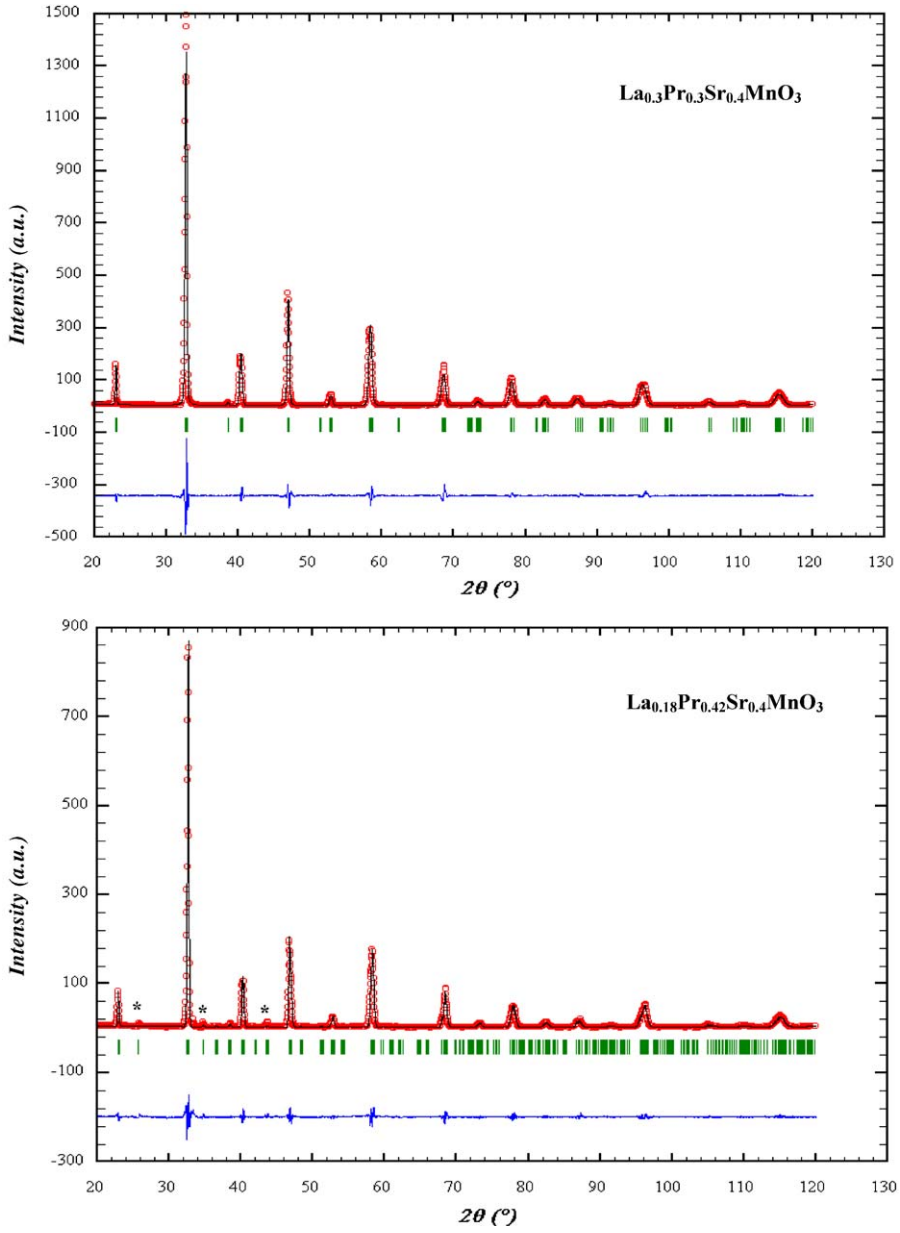

Fig. 2. Observed (open symbols) and calculated (solid lines) X-ray diffraction pattern for $La_{0.6-x}Pr_xSr_{0.4}MnO_3$ ($x = 0.3$ and 0.42). Positions for the Bragg reflection are marked by vertical bars. Differences between the observed and the calculated intensities are shown at the bottom of the diagram.

exists for our samples we have measured the magnetization with a Foner magnetometer equipped with a super conducting coil in magnetic field for $x = 0.6$ from 10 to 340 K in the temperature range. These measurements reveal a small drop of the magnetization below 150 K with a magnetic field of 500 Oe for the $Pr_{0.6}Sr_{0.4}MnO_3$ compound as shown in Fig. 8. This phenomenon may be due to a canted spin-state or mixture of magnetic phases below 150 K, and may be also due to a structural transition [21]. It also appears a small anomaly at 50 K, which may be due to the experiment.

5. Electrical properties

The variation of the resistivity versus temperature measured with the four-probe technique in the earth's magnetic field is represented in Fig. 9.

In the low temperature ferromagnetic regime, the temperature dependence of the resistivity for all the samples can be well expressed by the relation $\rho(T) = \rho(0) + AT^2$ ($T \leqslant 230$ K) as shown in Fig. 10. These results suggest that the electron–electron scattering process associated to spin fluctuation plays an important role in the present manganese oxides [22,23].

Using the sign of the temperature coefficient of resistivity ($d\rho/dT$) as a criterion, we found that for $0 \leqslant x \leqslant 0.6$, these compounds are ferromagnetic-metallic at low temperature ($T < T_p$) and become paramagnetic-semiconductor above the temperature peak T_p indicated by arrow. The conduction in the ferromagnetic phase ($T < T_p$) is generally understood according to the DE theory. The Mn^{3+}–O–Mn^{4+} coupling produces conduction through charge transfer from the half-filled to empty e_g orbital. The resistivity transition temperature T_p decreases from 350 to 280 K and the maximum of the resistivity, $\rho(T_p)$ increases with increasing x.

The A coefficient and the resistivity at T_p as a function $\langle r_A \rangle$ in the range 1.231–1.254 Å are given in Fig. 11. The remarkable phenomenon is the observation of the correlation between A and $\rho(T_p)$ reflecting that a strong electron correlation would be inherent in the present manganites system, even at temperatures up to T_p [24]. We note also that A and $\rho(T_p)$ sharply decrease when $\langle r_A \rangle$ increases. The origin of this phenomenon can be interpreted in terms of the structural phase transition from rhombohedral to orthorhombic. At high temperature, in the paramagnetic phase (T_p), the conduction is thermally activated indicating a conduction by magnetic polaron.

For samples with $x = 0$, 0.18, 0.3, 0.54 and 0.6, the resistivity obeys above T_p the standard relation:

$$\rho = \rho_0 \exp(E_{hop}/kT),$$

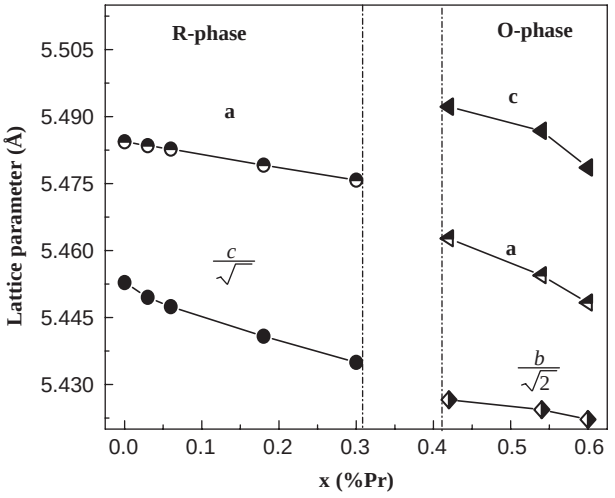

Fig. 3. Variation of lattice parameters with x for $La_{0.6-x}Pr_xSr_{0.4}MnO_3$.

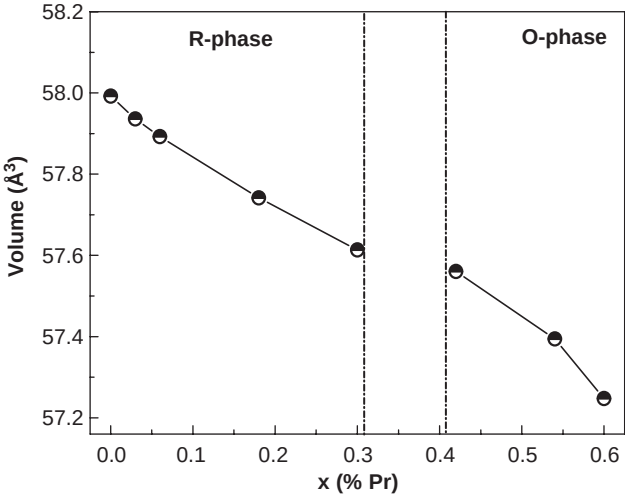

Fig. 4. Variation of unit cell volume with x for $La_{0.6-x}Pr_xSr_{0.4}MnO_3$.

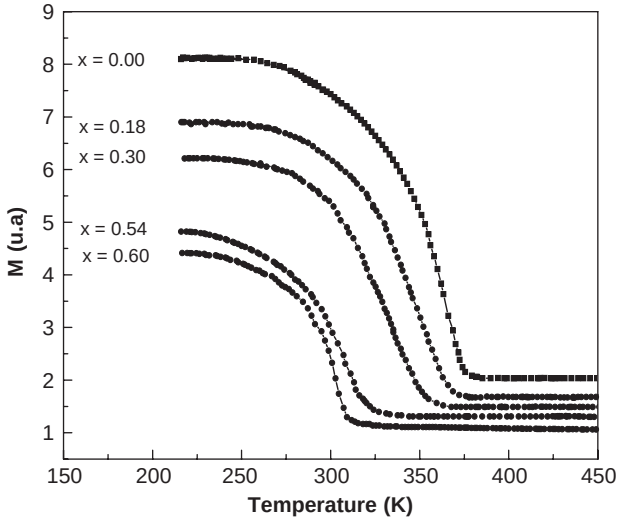

Fig. 5. Magnetization of $La_{0.6-x}Pr_xSr_{0.4}MnO_3$ as a function of temperature measured at $H = 500$ Oe.

Table 2
Values of average distance and angle in $La_{0.6-x}Pr_xSr_{0.4}MnO_3$

x	0	0.03	0.06	0.18	0.3	0.42	0.54	0.6
Structure	Rhombo	Rhombo	Rhombo	Rhombo	Rhombo	Ortho	Ortho	Ortho
d_{Mn-OI} (A°)	1.9440(5)	1.9445(1)	1.9447(2)	1.9450(1)	1.9458(4)	1.962(3)	1.958(4)	1.955(7)
d_{Mn-OII} (A°)	—	—	—	—	—	1.972(3)	1.956(3)	1.954(6)
	—	—	—	—	—	1.931(7)	1.938(3)	1.977(5)
$\theta_{Mn-OI-Mn}$ (°)	168.92(1)	168.41(1)	168.19(5)	167.19(4)	165.68(6)	165.05(5)	162.53(2)	160.60(6)
$\theta_{Mn-OII-Mn}$ (°)	—	—	—	—	—	168.31(1)	166.96(4)	166.27(5)
$\langle r_A \rangle$ (Å)	1.254	1.252	1.251	1.247	1.242	1.238	1.233	1.231

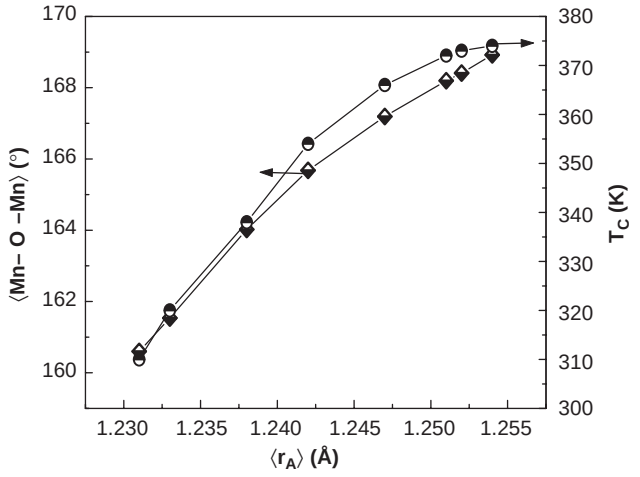

Fig. 6. Variation of bond angle Mn–O–Mn and T_C with $\langle r_A \rangle$ for $La_{0.6-x}Pr_xSr_{0.4}MnO_3$.

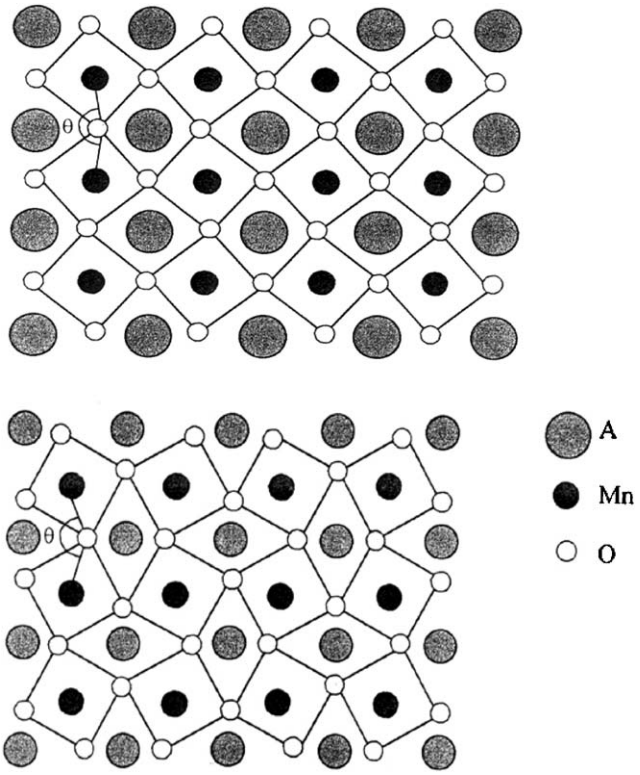

Fig. 7. The Mn–O–Mn bond angle in different distorted perovskite structure projected in the $(\vec{a},\vec{b})$ plane.

where ρ_0 is a pre-exponential coefficient and E_{hop} is the hopping energy. Form the linear part of the curves $\mathrm{Log}(\rho) - 1/T$ (Fig. 11 inset), we deduce that the values of E_{hop} increase from 19.16 meV for $x = 0$ to 86.9 meV for $x = 0.6$. The difference in the E_{hop} values may be related to the existence of two structures.

Table 3
Variation of Curie temperature transition T_C with cation-size variance σ^2 for three samples with constant $\langle r_A \rangle = 1.248$ Å and $Mn^{3+}/Mn^{4+} = 3/2$

Samples	σ^2 (Å^2)	T_C (K)
$La_{0.6}Sr_{0.36}Ca_{0.04}MnO_3$ [17]	0.00218	363
$La_{0.46}Pr_{0.14}Sr_{0.4}MnO_3$ (Present work)	0.00272	368
$La_{0.2}Nd_{0.4}Pb_{0.4}MnO_3$ [18]	0.00725	270

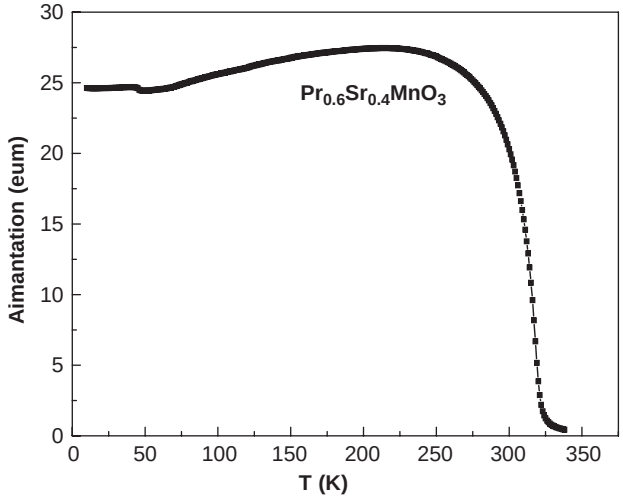

Fig. 8. Variation of magnetization measured with the Foner magnetometer as a function of temperature for $x = 0.6$.

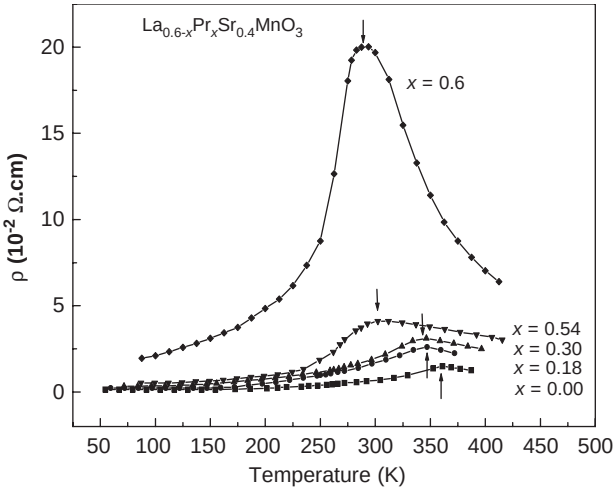

Fig. 9. Temperature dependence of the resistivity for $La_{0.6-x}Pr_xSr_{0.4}MnO_3$.

6. Conclusion

In this work, we have investigated the structure, magnetic and electrical properties of perovskite $La_{0.6-x}Pr_xSr_{0.4}MnO_3$

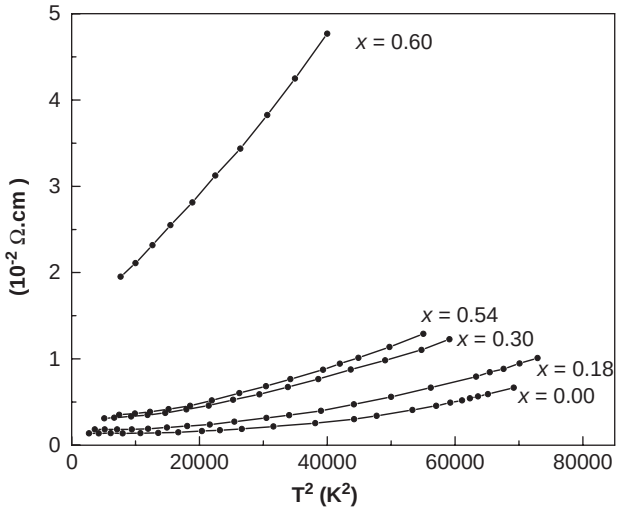

Fig. 10. Temperature dependence of resistivity in the low-temperature ferromagnetic regime.

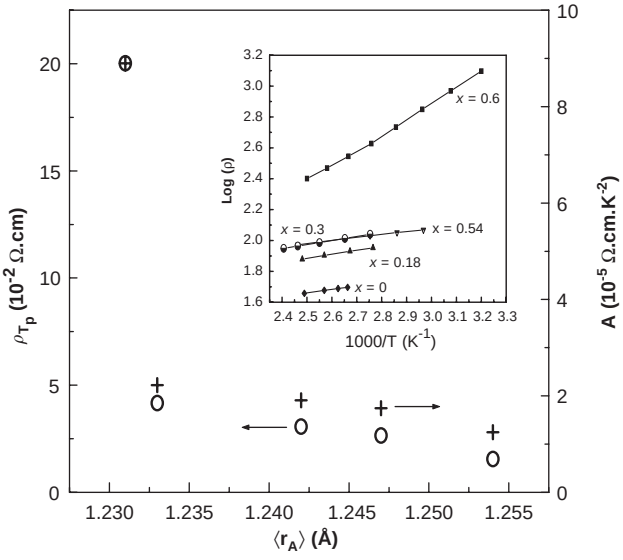

Fig. 11. The resistivity at $T_p(\rho T_p)$ and the coefficient A as a function of $\langle r_A \rangle$ for $La_{0.6-x}Pr_xSr_{0.4}MnO_3$.

compounds. These compounds exist in a single-phase at room temperature having a rhombohedral structure for $1.242\,\text{Å} \leqslant \langle r_A \rangle \leqslant 1.254\,\text{Å}$ and an orthorhombic structure for $1.231\,\text{Å} \leqslant \langle r_A \rangle \leqslant 1.238\,\text{Å}$. These samples present a single transition from a ferromagnetic metallic to a paramagnetic insulating phase. The unit cell volume and the Curie temperature increase with $\langle r_A \rangle$, so that the maximum of the resistivity $\rho(T_\rho)$ decreases when the average size of the A-site cations $\langle r_A \rangle$ increases. These variations can be interpreted by the change of the Mn–O–Mn bond angle when $\langle r_A \rangle$ decreases.

References

[1] E.O. Wollan, W.C. Koehler, Phys. Rev. 100 (1955) 545.
[2] G.H. Jonker, Physica 22 (1956) 707.
[3] Y. Tokura, A. Urushibara, Y. Moritoma, T. Arima, J. Phys. Soc. Japan 63 (1994) 3991.
[4] L. Righi, P. Gorria, M. Insausti, J. Gutiérrez, J.M. Barandiaran, J. Appl. Phys. 81 (1997) 5767.
[5] A. Maignan, F. Damay, C. Martin, B. Raveau, Mater. Res. Bull. 32 (1997) 965.
[6] Z. Jirak, F. Damay, M. Hervieu, C. Martin, Phys. Rev. B 61 (2000) 1181.
[7] C. Zener, Phys. Rev. 82 (1951) 403.
[8] P.G. de Gennes, Phys. Rev. 118 (1960) 141.
[9] P.W. Anderson, H. Hasegawa, Phys. Rev. 100 (1955) 675.
[10] K. Kubo, N. Ohata, J. Phys. Soc. Japan 33 (1972) 21.
[11] H.Y. Hwang, S.W. Cheong, P.G. Radalli, Phys. Rev. Lett. 75 (1995) 914.
[12] Z.B. Guo, N. Zhang, W.P. Ding, W. Yang, Solid State Commun. 100 (1996) 769.
[13] H.M. Rietveld, J. Appl. Crystallogr. 2 (1969) 65.
[14] R.D. Shannon, Acta Crystallogr. Sect. A 32 (1976) 751.
[15] L.M. Rodriguez-Martinez, J.P. Attfield, Phys. Rev. B 54 (1996) 15622.
[16] F. Damay, C. Martin, A. Maignan, B. Raveau, J. Appl. Phys. 82 (12) (1997) P6182.
[17] N. Abdelmoula, J. Dhahri, K. Guidara, E. Dhahri, J.C. Joubert, Phase Transitions 70 (1999) 211–222.
[18] D.W. Visser, A.P. Ramirez, M.A. Subramanian, Phys. Rev. Lett. 78 (1997).
[19] F. Damy, A. Megnan, C. Martin, B. Raveau, J. Appl. Phys. 81(3) (1997).
[20] J. Wolfman, Ch. Simon, M. Hervieu, A. Maignan, B. Raveau, J. Solid. State Chem. 123 (1996) 413.
[21] Gen. Matsumoto, J. Phys. Soc. Japon 29 (1970) P620.
[22] A. Urushibara, Y. Moritomo, T. Arima, A. Asamitsu, G. Kido, Y. Tokura, Phys. Rev. B 51 (1995) 14103.
[23] E. Inaba, T. Arima, T. Ishikawa, T. Katsufigi, Y. Tokura, Phys. Rev. B 52 (1995) 2221.
[24] Z. Guo, J. Zhang, W. Ding, H. Huang, Y. Du, Appl. Phys. Lett. 70 (14) (1997) 1897.